Organic Electronics 80 (2020) 105613

Contents lists available at ScienceDirect

Organic Electronics

journal homepage: http://www.elsevier.com/locate/orgel

Stability enhancement of inverted perovskite solar cells using LiF in electron transport layer

Dawei Tan [a,b,1], Xuejing Zhang [a,b,1], Xiao Liu [a,b], Hongmei Zhang [a,b,*], Dongge Ma [c,**]

[a] Key Laboratory for Organic Electronics and Information Displays & Jiangsu Key Laboratory for Biosensors, Nanjing University of Posts & Telecommunications (NUPT), Nanjing, 210023, PR China

[b] Jiangsu National Synergetic Innovation Center for Advanced Materials (SICAM), Nanjing University of Posts & Telecommunications (NUPT), Nanjing, 210023, PR China

[c] Institute of Polymer Optoelectronic Materials and Devices, State Key Laboratory of Luminescent Materials and Devices, South China University of Technology, Guangzhou, 510640, PR China

ARTICLE INFO

Keywords:
LiF
Stability
Perovskite solar cells

ABSTRACT

Stability is of great importance to the commercialization of perovskite solar cells (PVSCs). Interface materials are crucial to achieve stable PVSCs. Herein, we report on a strategy of incorporating lithium fluoride (LiF) as part of the buffer layer in inverted PVSCs to suppress the decomposition of perovskite layer and eliminate the corresponding negative effects. The device with C_{60}/LiF buffer layer maintains 87% of its initial efficiency after aging in N_2 for 26 days, exhibiting much improved stability compared to the control device with C_{60}/BCP. Our work suggests a viable approach to enhance the device stability for the commercialization of PVSCs.

1. Introduction

Organic-inorganic hybrid lead halide perovskite solar cells (PVSCs) have been attracting intensive interest in the past years with power conversion efficiencies (PCEs) evolving from 3.8% in 2009 to a certified 25.2% in 2019 [1,2], making them a promising alternative to conventional thin film solar cells. The efficiency has been comparable with that of commercial thin film solar cells [3,4], however, the major challenge for commercialization is its long-term environmental stability. To be specific, perovskite materials suffer from rapid degradation upon exposure to humidity [5].

In order to improve the stability, great progress has been made in various device configurations, including the classic mesoporous n-i-p and the mesoporous-free inverted p-i-n planar configurations. Typically, the inverted planar devices have a structure of indium tin oxide (ITO)/poly (3,4-ethylene -dioxythiophene):poly- (styrenesulfonate) (PEDOT:PSS)/peorvskite/[6,6]-phenylC61-butyric acid methyl ester (PCBM)/cathode. It has attracted considerable attention due to its low-temperature process and small hysteresis effect. However, low work function (WF) metals such as Al (~4.1 eV) or Ag (~4.8 eV) often used as cathode electrode for efficient electron extraction are susceptible to be corroded by components from decomposed perovskite layer [6–8], causing instable devices. The choice of top electron transport layer (ETL) in the inverted p-i-n planar PVSCs plays an important role in the stability improvement since it can provide a blocking function to prevent the reaction between metal cathode and underlying perovskite layer. Therefore, a suitable cathode buffer layer is crucial to the performance of planar PSCs. A variety of cathode buffer layers including organic and inorganic materials such as bathocuproine (BCP), SnO_2 and aluminum-doped zinc oxide (AZO), have been inserted between PCBM and top metal electrode to improve both efficiency and stability [9–11]. Lithium fluoride (LiF) is capable of preventing ion and moisture through metal cathode into photoactive layer in organic photovoltaics (OPVs) [12]. Although LiF works as an effective interfacial layer in inverted p-i-n planar PVSCs [13–17], it lacks the investigation on the effect of LiF on performance stability [18–21].

Herein, we report on the incorporation of LiF as part of the buffer layer in inverted PVSCs to improve the device stability. We used C_{60}/LiF bilayer to prevent decomposition of perovskite layer and reduce the negative influence. As a result, the device with C_{60}/LiF keeps 87% of its

* Corresponding author. Key Laboratory for Organic Electronics and Information Displays & Jiangsu Key Laboratory for Biosensors, Nanjing University of Posts & Telecommunications (NUPT), Nanjing, 210023, PR China.

** Corresponding author.

E-mail addresses: iamhmzhang@njupt.edu.cn (H. Zhang), msdgma@scut.edu.cn (D. Ma).

[1] These authors contributed equally.

https://doi.org/10.1016/j.orgel.2019.105613
Received 15 September 2019; Received in revised form 9 December 2019; Accepted 28 December 2019
Available online 30 December 2019

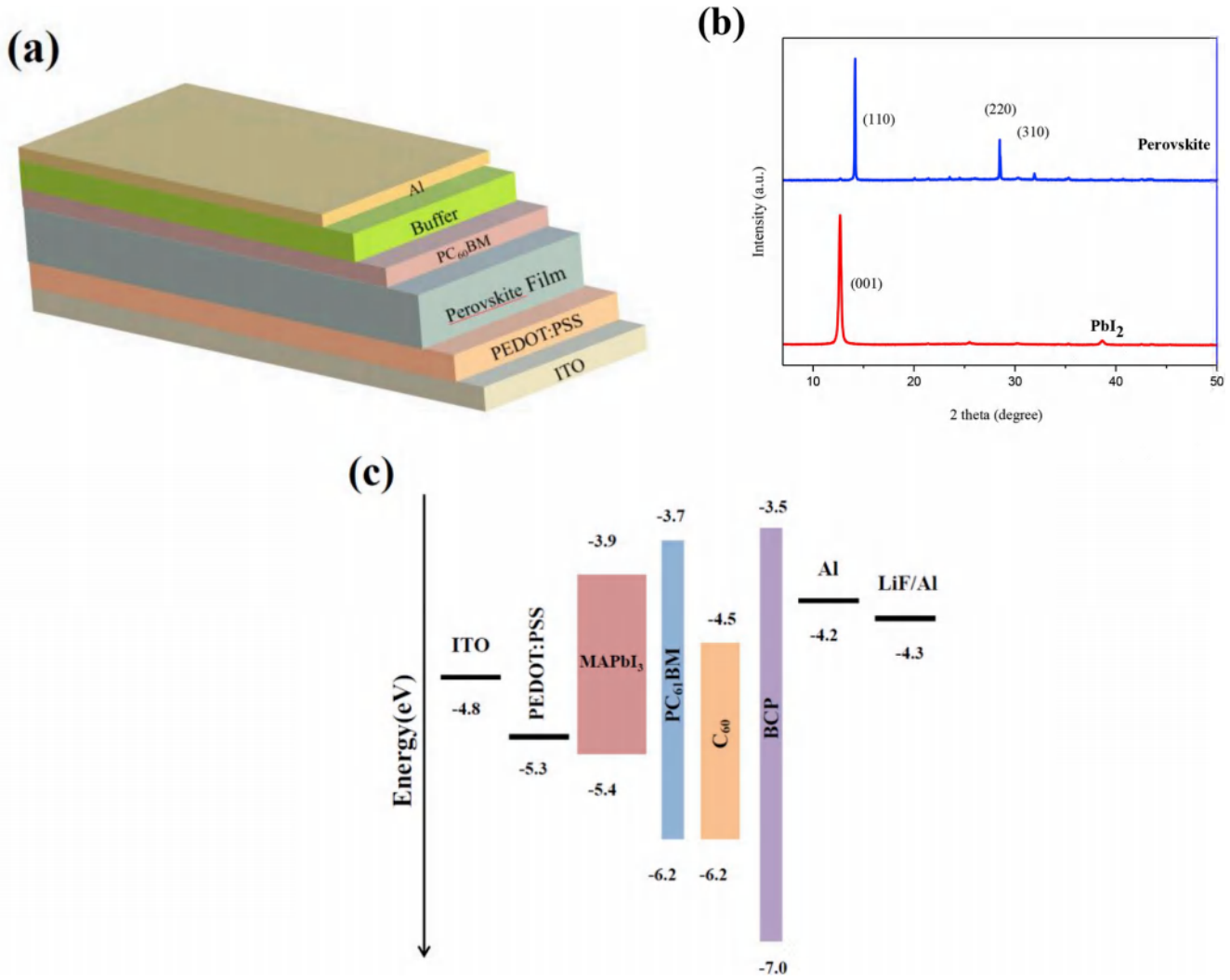

Fig. 1. (a) Schematic of device architecture. (b) XRD patterns of PbI_2 and perovskite film. (c) band alignment diagram.

initial efficiency after storage in N_2 for 26 days, reflecting obvious stability improvement compared with the control one without LiF included.

2. Experimental section

2.1. Materials

PEDOT:PSS (CLevios PVP Al4083) was obtained from Heraeus Inc. CH_3NH_3I (≥99.5%), PbI_2(≥99.999%), fullerene (C_{60}, ≥99.5%), LiF (≥99.85%) were obtained from Alfa Aesar. $PC_{61}BM$ (≥99.5%) was purchased from Organtec Materials Inc. BCP (≥98%) was purchased from Jilin OLED Material Tech Co., Ltd. Inc. Isopropyl alcohol (IPA) (≥99.5%), N,N-dimethylformamide (DMF) (≥99.5%), 1,2-dichlorobenzene (≥99.5%), acetone (≥99.5%) and absolute ethanol (≥99.7%) were purchased from Sinopharm Chemical Reagent Co., Ltd. All materials were used as purchased.

2.2. Device fabrication

The ITO-coated glass substrates were cleaned with detergent, deionized water, acetone and ethanol in ultrasonic bath (Shu-mei KQ300DE) for 15 min, respectively, and then treated with UV-ozone for 15 min. PEDOT:PSS aqueous solution filtered through a 0.45 μm filter was spin-coated onto ITO substrate at 3500 rpm for 60 s, followed by annealing at 120 °C for 15 min. The coated substrates were then transferred to a nitrogen-filled glove-box (both H_2O and $O_2 < 0.1$ ppm). We used a two-step deposition method to prepare perovskite layer. PbI_2 solution in DMF (1 mol/L) was spin-coated on top of PEDOT:PSS. Before the PbI_2 layer was fully dried, a fresh CH_3NH_3I (MAI) solution in IPA (50 mg/mL) was spin-coated onto the as-prepared PbI_2 layer at 6000 rpm for 35 s immediately, followed by a thermal annealing at 100 °C for 15 min. The ETL was prepared by using 20 mg/mL $PC_{61}BM$ in 1,2-dichlorobenzene at 6000 rpm for 15 s. Finally, C_{60} (20 nm), LiF (1 nm) or BCP (10 nm), Al (120 nm) layers were sequentially deposited on top of the perovskite film by thermal evaporation under vacuum (10^{-6} mbar) through a shadow mask with an active area of 0.11 cm^2.

2.3. Film and device characterizations

The current density-voltage (*J-V*) curves of the PVSCs were measured using a Keithley 2400 source meter under 100 mW/cm^2 illumination of simulated AM 1.5G sunlight certified to the JIS C 8912 standard. The X-ray diffraction (XRD) patterns of PbI_2 and perovskite on ITO/PEDOT:PSS substrates were examined by D/Max-3A diffractometer (RIGAKU, Japan) with Cu Kα irradiation at the 2θ range of 10–50°. The Electrochemical Impedance Spectroscopy (EIS) measurements were performed on a CHI660 electrochemical workstation (CH Instrument Inc.). A 10 mV voltage perturbation was applied at different dc voltages ranging from 0 to V_{oc} with frequencies between 5 and 10^5 Hz under dark condition. All devices were measured under the ambient air condition.

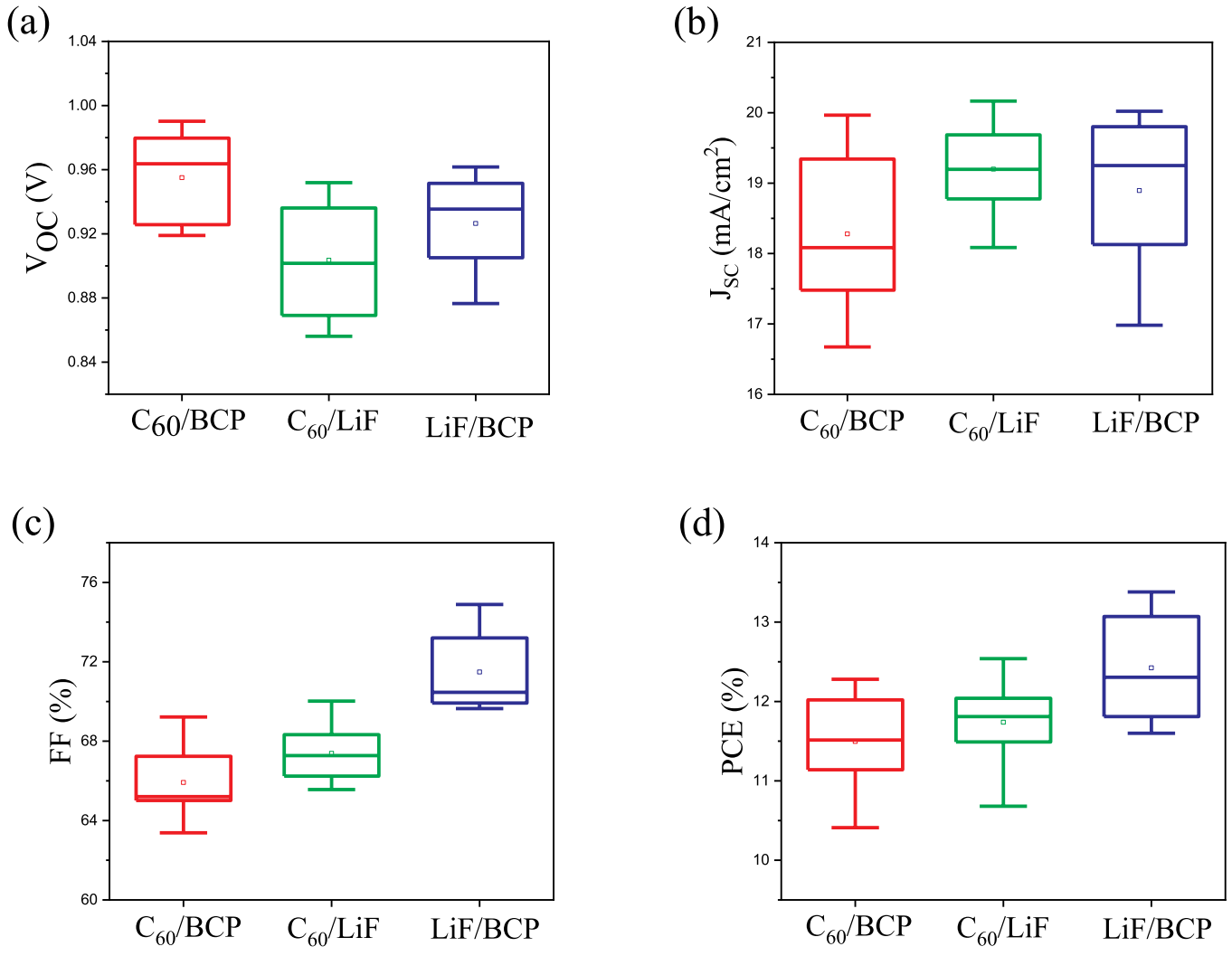

Fig. 2. (a) V_{OC}, (b) J_{SC}, (c) FF, and (d) PCE distribution of PVSCs with different buffer layer combination.

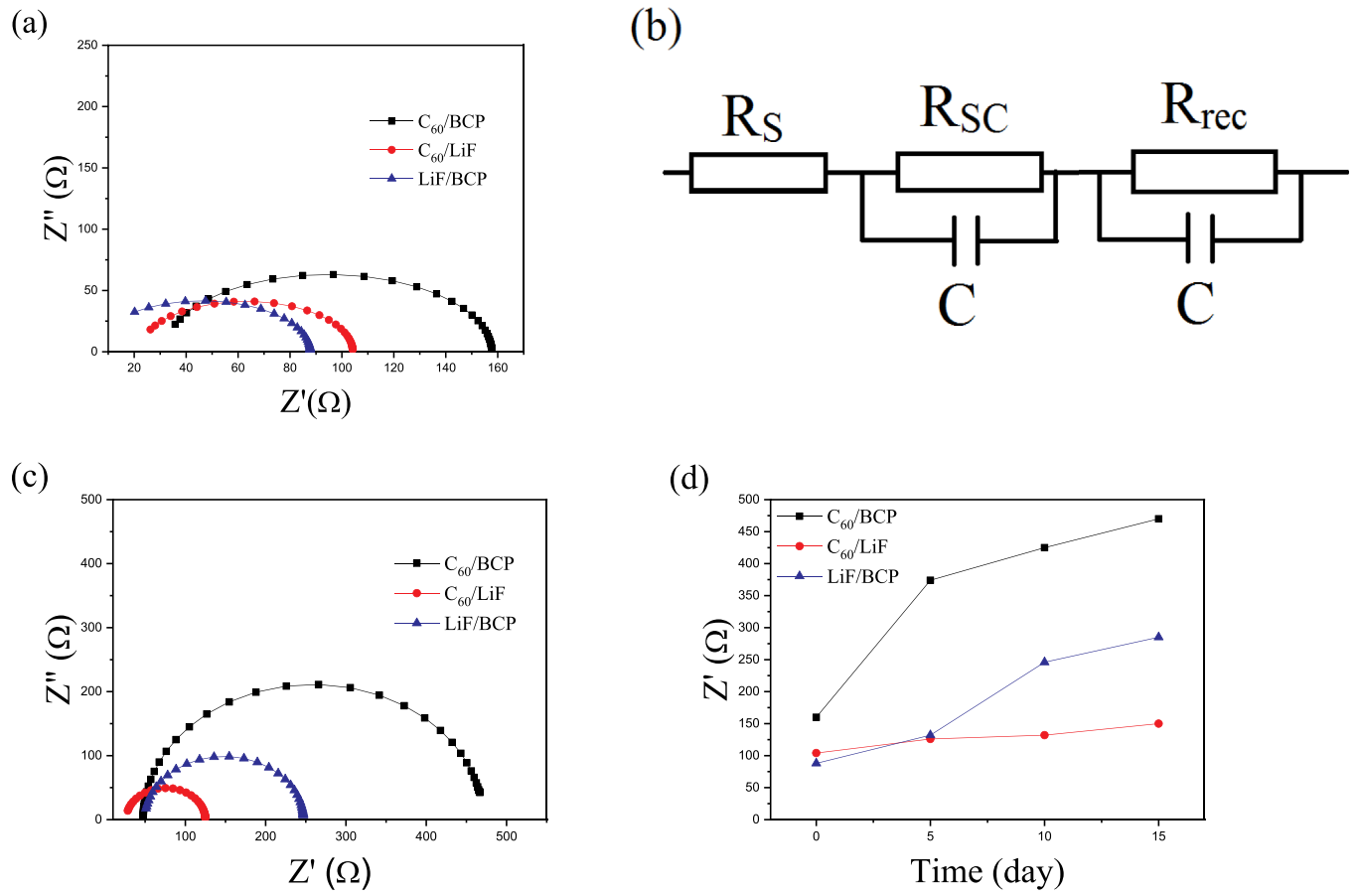

Fig. 3. Nyquist plots of $CH_3NH_3PbI_3$ PVSCs with different buffer layer measured at V=V_{OC} under dark condition. (a) as-prepared devices, (b) The equivalent circuit model for fitting the plots, (c) the devices aged for 15 days, (d) statistics numerical values for R_{sc} based on different buffer layer.

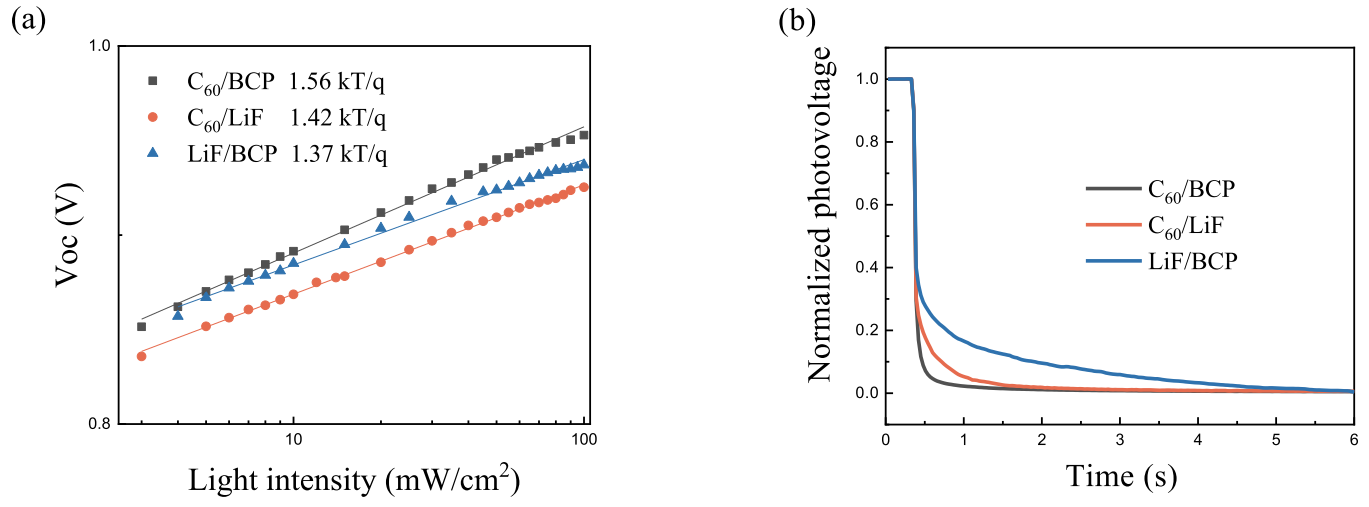

Fig. 4. (a) V_{oc}-light intensity dependence of, (b) transient photovoltage decay of devices with different buffer.

3. Results and discussion

The device architecture and band alignment diagram are illustrated in Fig. 1a,c. We used PEDOT:PSS and $PC_{61}BM$ as HTL and ETL, respectively. Buffer layer consists of C_{60}/BCP, C_{60}/LiF, or LiF/BCP. Observed from the XRD patterns (Fig. 1b), the $MAPbI_3$ perovskite film exhibits main diffraction peaks at around 14.16° and 28.48°corresponding to the (110) and (220) crystal planes, respectively, consistent with the previous report [22]. The peak at 12.0° corresponding to PbI_2 almost disappears.

In order to investigate the effect of LiF on the device stability, the devices with a dual buffer layer such as C_{60}/LiF or LiF/BCP were compared with the control device with C_{60}/BCP ETL. We do see the large variation on the performance of these devices. Fig. 2 shows photovoltaic parameter distribution of PVSCs with different buffer layers measured under AM1.5 simulated sunlight. It is clear that PVSCs fabricated with C_{60}/BCP ETL display an average V_{OC} of 0.95 V, a J_{SC} of 18.27 mA/cm^2, a FF of 65.92%, and a PCE of 11.49%. By replacing BCP with LiF, the

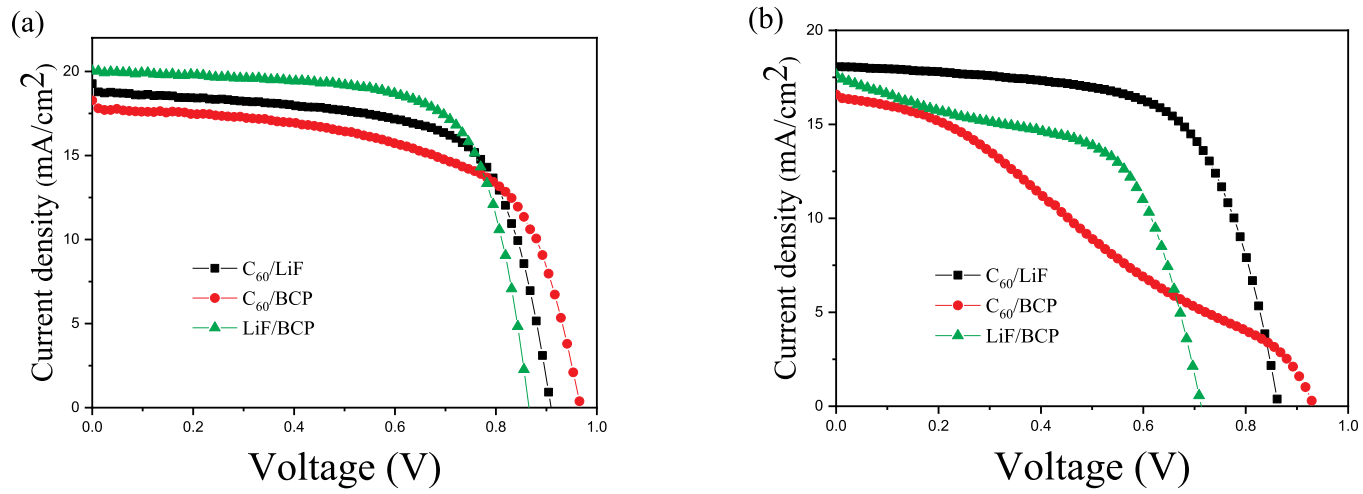

Fig. 5. *J-V* curves of PVSCs with different buffer layers stored for (a) 0 day and (b) 26 day.

average V_{OC} decreases to 0.90 V, along with J_{SC} and FF increasing to 19.19 mA/cm^2 and 67.38%, leading to an approximate PCE of 11.73%. However, PVSCs with LiF/BCP buffer display remarkable increase in the average FF of 71.48%, and slightly lower V_{OC} and J_{SC} of 0.93 V and 18.89 mA/cm^2, respectively. As a result, the highest PCE of 13.38% is achieved.

We characterized and analyzed the effect of different buffer layers on photovoltaic performance by EIS. Fig. 3 exhibits the Nyquist plots of the as-prepared PVSC with different buffer layers measured under dark condition at a bias voltage of V=V_{OC}, and the semicircle arc is typically related to the interfacial charge transfer process which is ascribed to the contact resistance (R_{SC}) in the devices [7]. The R_{SC} evaluates the selective contacts and the interface correlated with the FF. As shown in Fig. 3, the R_{SC} of PVSC with C_{60}/BCP, C_{60}/LiF and LiF/BCP is 157.6, 104.1, and 87.8 Ω/cm^2, respectively. Incorporation of LiF in the buffer layer leads to significant decrease in R_{SC}, indicating that LiF forms a preferable contact and interface with perovskite active layer, especially in the case of LiF/BCP, corresponding to the increase in the FF as shown in Fig. 2c.

As reported [23–25], lithium salt promotes device performance by affecting electron properties of ETL. We then investigated charge recombination kinetics by measuring the dependence of V_{oc} on light intensity and transient photovoltage decay as shown in Fig. 4. The slope of V_{oc}-light intensity dependence in Fig. 4a is relative to the trap-assisted recombination and defined as the ideal factor [26,27]. Device with LiF/BCP buffer exhibits the smallest slope of 1.37 kT/q while devices with C_{60}/LiF and C_{60}/BCP show larger slopes of 1.42 kT/q and of 1.56 kT/q, respectively. This implies a reduced Shockley-Read-Hall recombination by LiF. We also performed transient photovoltage decay to probe the charge recombination with different buffers. As shown in Fig. 4b, the control device with C_{60}/BCP shows a rapid drop of V_{oc} value. However, the device with C_{60}/LiF has a slower decay and the device with LiF/BCP shows the slowest decay of V_{oc}, suggesting the alleviated non-radiative recombination [26,27]. These are in agreement with the trend of the FF.

We then discussed the distinct effect of different buffer layer combination on the device stability. The encapsulated devices were stored in N_2-filled glove-box and measured every few days under AM 1.5G simulated solar irradiation (100 mW/cm^2) in ambient. Fig. 5a and b show the *J-V* curves of the devices with different buffer layer that were as-prepared and aged for 26 days, respectively. The *J-V* curves of the as-prepared devices show coincident arc. After storage for 26 days, the *J-V* curve of the cell with C_{60}/LiF keeps original shape, and however those of the cells with C_{60}/BCP and LiF/BCP change largely.

The main photovoltaic parameters of the three types of devices with aging time were summarized in Table 1 and plotted in Fig. 6a–d. The device with C_{60}/LiF maintains 87% of its initial efficiency after being stored in N_2 for 26 days, while the device with C_{60}/BCP has only 42% of its initial efficiency during this duration. The primary change of the device with C_{60}/BCP is the FF, quickly decreasing to 48% of the initial FF values after aging for 26 days. By contrast, the device with C_{60}/LiF still retains more than 95% of its initial FF value. This result suggests that the enhanced stability could be attributed to incorporation of LiF in the buffer layer. However, it is worth mentioning that the device with LiF/BCP shows unsatisfied stability which retains 58% after 26-day aging, exhibiting that both J_{SC} and FF of the device with LiF/BCP decrease, while the other two devices with C_{60} as part of the buffer layer show stable J_{SC}. On one hand, C_{60} is hydrophobic owing the low surface energy which is helpful to protect perovskite [25,28]. On the other hand, C_{60}^8 is well accepted to enable the passivation on defects [29] and thus the device performance is kept for a longer time. However, the hydrophilic LiF is too thin to perform the same function.

In order to get deep insight into the stability improvement, electrochemical impedance spectroscopy (EIS) was employed to study the degradation process. Fig. 3c shows the Nyquist plots of the PVSC with different buffer layers aged for 15 days and R_{SC} values obtained with the bias voltage at V=V_{OC} were summarized in Fig. 3d. It is apparent that

Table 1
Summary on the main photovoltaic parameters of the three types of devices with aging time.

Layer	Time (day)	V_{OC} (V)	J_{SC} (mA/cm^2)	FF	PCE (%)
C_{60}/LiF	0	0.9091	18.8759	67.45	11.57
	4	0.9002	18.9129	67.39	11.47
	8	0.8992	18.8044	67.06	11.34
	12	0.8801	18.5875	65.66	10.74
	16	0.8671	18.4655	64.24	10.29
	20	0.8515	18.5051	63.98	10.08
	24	0.8578	17.8655	65.65	10.06
	26	0.8639	18.1454	64.72	10.15
C_{60}/BCP	0	0.9675	17.8703	61.9	10.70
	4	0.9451	16.8716	62.16	9.91
	8	0.9336	17.4216	57.58	9.37
	11	0.9267	17.5048	50.74	8.23
	14	0.9222	17.2868	44.89	7.16
	17	0.9231	16.8324	38.10	5.92
	20	0.9304	16.3056	32.84	4.98
	23	0.9207	16.5237	30.35	4.62
	26	0.9266	16.5093	29.71	4.54
LiF/BCP	0	0.8653	20.0175	70.18	12.16
	3	0.8058	19.7961	63.47	10.12
	6	0.8019	19.2980	61.92	9.58
	23	0.7245	17.7164	58.08	7.45
	26	0.7130	17.5527	57.09	7.15

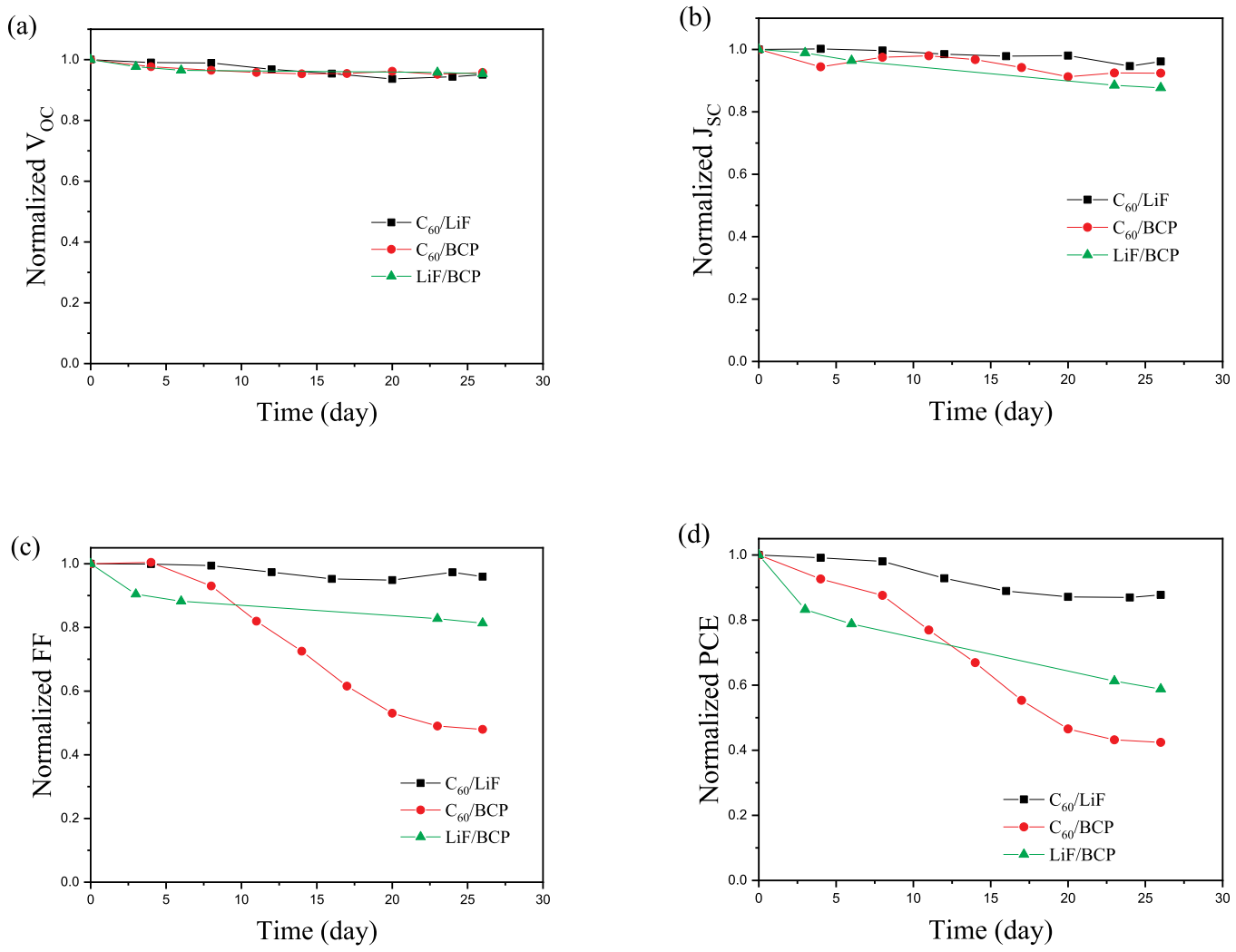

Fig. 6. Storage stability of the devices with different buffer layer with time. (a) V_{OC}, (b) J_{SC}, (c) FF, and (d) PCE.

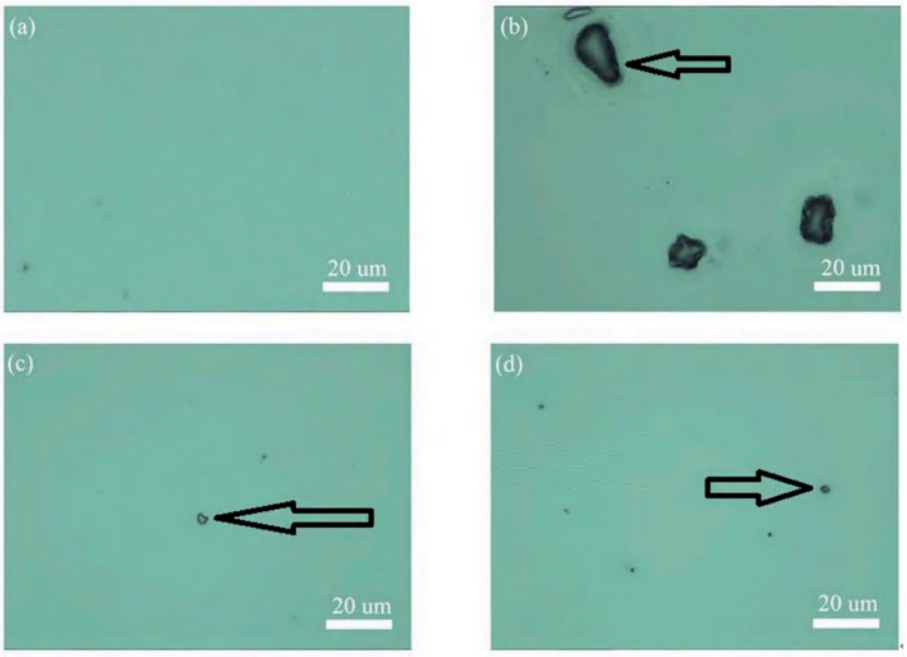

Fig. 7. The morphology image of Al electrode bubbles on PVSCs and stored in glove-box (H_2O < 0.1 ppm and O_2 < 0.1 ppm) for 0 or 10 days. (a) freshly prepared device, (b) device with C_{60}/BCP, (c) device with C_{60}/LiF, (d) device with LiF/BCP.

with the time increasing R_{SC} values of different devices become large. After aged for 15 days, the device with C_{60}/BCP shows largest R_{SC}, and meanwhile, the R_{SC} value of the device with LiF/BCP is higher than that of the device with C_{60}/LiF. Similarly, the R_{SC} of the device with C_{60}/BCP increases the most rapidly with the largest slope, while the device with LiF has a much stable change, indicating LiF makes the selective contact and interface relatively stable under the degradation process.

As reported [8], perovskite decomposes and generates gaseous products like HI, leading to formation of the voids in the charge transport layer and corrosion of metal electrode. This may account for the declined PCE and FF of our devices. The stable R_{SC} and FF with incorporating LiF in the buffer layer indicate that gaseous product HI could be isolated from cathode Al. To verify this assumption, optical microscope was performed to characterize the cathode surfaces of different types of devices with various buffer layer and the corresponding images are shown in Fig. 7. Obviously, the surface with LiF in the buffer layer has limited damages with tiny bubbles after stored for 10 days, as shown in Fig. 7c and d. However, in Fig. 7b, large bubbles are observed on the surface of the device with C_{60}/BCP, as a result of decomposed HI and CH_3NH_2(g) at the gas state. This result indicates that LiF is able to protect cathode Al from damage by decomposition products such as HI.

4. Conclusions

We have demonstrated the stability improvement of the PVSC performance by employing the LiF as part of the buffer layer, which protects the metal electrode from damage caused by the decomposition products from the perovskite layer and meanwhile maintains the relatively stable interface contact. The device with C_{60}/LiF buffer layer, maintaining 87% of its initial efficiency after aging in N_2 for 26 days, has much improved stability compared to that with C_{60}/BCP. Using LiF as the blocking layer, decomposition products are isolated from metal electrode, avoiding decomposition process. This work offers an effective strategy to improve the device stability of PVSC by incorporating LiF as part of buffer layer to perform dual function of preventing the decomposition and eliminating the effects of decomposition.

Declaration of competing interest

The authors declare that they have no known competing financial interests or personal relationships that could have appeared to influence the work reported in this paper.

Acknowledgements

The authors are thankful for the financial support of the grant from the National Natural Science Foundation of China (51333007) and Natural Basic Research Program of China (973 Program, 2015CB9322003).

References

[1] Nrel, Best research-cell efficiencies, Http://Www.Nrel.Gov,Accessed: August 2, 2019.'.
[2] A. Kojima, K. Teshima, Y. Shirai, T. Miyasaka, Organometal halide perovskites as visible-light sensitizers for photovoltaic cells, J. Am. Chem. Soc. 131 (2009) 6050.
[3] Jeffrey A. Christians, Philip Schulz, Jonathan S. Tinkham, Tracy H. Schloemer, Steven P. Harvey, Bertrand J. Tremolet de Villers, Alan Sellinger, Joseph J. Berry, Joseph M. Luther, Tailored interfaces of unencapsulated perovskite solar cells for >1,000 hour operational stability, Nature Energy 3 (2018) 68–74.
[4] Konrad Domanski, Essa A. Alharbi, Anders Hagfeldt, Michael Grätzel, Wolfgang Tress, Systematic investigation of the impact of operation conditions on the degradation behaviour of perovskite solar cells, Nature Energy 3 (2018) 61–67.
[5] J.L. Yang, B.D. Siempelkamp, D.Y. Liu, T.L. Kelly, Investigation of Ch3nh3pbi3 degradation rates and mechanisms in controlled humidity environments using in situ techniques, ACS Nano 9 (2015) 1955–1963.
[6] S. Yue, S. Lu, K. Ren, K. Liu, M. Azam, D. Cao, Z. Wang, Y. Lei, S. Qu, Z. Wang, Insights into the influence of work functions of cathodes on efficiencies of perovskite solar cells, Small 13 (2017).
[7] Chunhua Wang, Chujun Zhang, Yulan Huang, Sichao Tong, Han Wu, Jian Zhang, Yongli Gao, Junliang Yang, Degradation behavior of planar heterojunction Ch 3 Nh 3 pbi 3 perovskite solar cells, Synth. Met. 227 (2017) 43–51.
[8] Y. Han, S. Meyer, Y. Dkhissi, K. Weber, J.M. Pringle, U. Bach, L. Spiccia, Y. B. Cheng, Degradation observations of encapsulated planar Ch3nh3pbi3 perovskite solar cells at high temperatures and humidity, J. Mater. Chem. 3 (2015) 8139–8147.
[9] Chuanliang Chen, Shasha Zhang, Shaohang Wu, Wenjun Zhang, Hongmei Zhu, Zhenzhong Xiong, Yanjun Zhang, Wei Chen, Effect of Bcp buffer layer on eliminating charge accumulation for high performance of inverted perovskite solar cells, RSC Adv. 7 (2017) 35819–35826.
[10] Z. Zhu, Y. Bai, X. Liu, C.C. Chueh, S. Yang, A.K. Jen, Enhanced efficiency and stability of inverted perovskite solar cells using highly crystalline Sno2 nanocrystals as the robust electron-transporting layer, Adv. Mater. 28 (2016) 6478–6484.
[11] H. Dong, S. Pang, Y. Zhang, D. Chen, W. Zhu, H. Xi, J. Chang, J. Zhang, C. Zhang, Y. Hao, Improving electron extraction ability and device stability of perovskite solar cells using a compatible pcbm/azo electron transporting bilayer, Nanomaterials (Basel) 8 (2018).
[12] Xi Xi, Qinglei Meng, Fangxin Li, Yuqiang Ding, Jingjia Ji, Zhengrong Shi, Guohua Li, The characteristics of the small molecule organic solar cells with pedot: pss/Lif double anode buffer layer system, Sol. Energy Mater. Sol. Cells 94 (2010) 623–628.
[13] Xiaodong Liu, Ming Lei, Yi Zhou, Bo Song, Yongfang Li, High performance planar P-I-N perovskite solar cells with crown-ether functionalized fullerene and lif as double cathode buffer layers, Appl. Phys. Lett. 107 (2015), 063901.
[14] J. Seo, S. Park, Y.C. Kim, N.J. Jeon, J.H. Noh, S.C. Yoon, S.I. Sang, Benefits of very thin Pcbm and Lif layers for solution-processed P-I-N perovskite solar cells', Energy Environ. Sci. 7 (2014) 2642–2646.
[15] Kuan Sun, Jingjing Chang, Furkan Halis Isikgor, Pengcheng Li, Jianyong Ouyang, Efficiency enhancement of planar perovskite solar cells by adding zwitterion/Lif double interlayers for electron collection, Nanoscale 7 (2014) 896–900.
[16] X. Liu, H. Yu, L. Yan, Q. Dong, Q. Wan, Y. Zhou, B. Song, Y. Li, Triple cathode buffer layers composed of Pcbm, C60, and Lif for high-performance planar perovskite solar cells, ACS Appl. Mater. Interfaces 7 (2015) 6230–6237.
[17] X. Liu, L.J. Guo, Y. Zheng, 5-Nm Lif as an efficient cathode buffer layer in polymer solar cells through simply introducing a C60 interlayer, Nanoscale Res. Lett. 12 (2017) 543.
[18] Chenxin Ran, Jun Xi, Weiyin Gao, Fang Yuan, Ting Lei, Bo Jiao, Xun Hou, Zhaoxin Wu, Bilateral interface engineering toward efficient 2d–3d bulk heterojunction tin halide lead-free perovskite solar cells, ACS Energy Lett. 3 (2018) 713–721.
[19] Um Kanta Aryal, Veera Murugan Arivunithi, Saripally Sudhaker Reddy, Junyoung Kim, Yeong-Soon Gal, Sung-Ho Jin, Efficient dual cathode interfacial layer for high performance organic and perovskite solar cells, Org. Electron. 63 (2018) 222–230.
[20] S.J. Yuan, J. Wang, K.L. Yang, P.F. Wang, X. Zhang, Y.Q. Zhan, L.R. Zheng, High efficiency mapbi(3-X)Cl(X) perovskite solar cell via interfacial passivation, Nanoscale 10 (2018) 18909–18914.
[21] S. Pisoni, M. Stolterfoht, J. Lockinger, T. Moser, Y. Jiang, P. Caprioglio, D. Neher, S. Buecheler, A.N. Tiwari, On the origin of open-circuit voltage losses in flexible N-I-P perovskite solar cells, Sci. Technol. Adv. Mater. 20 (2019) 786–795.
[22] J. Burschka, N. Pellet, S.J. Moon, R. Humphry-Baker, P. Gao, M.K. Nazeeruddin, M. Gratzel, Sequential deposition as a route to high-performance perovskite-sensitized solar cells, Nature 499 (2013) 316–319.
[23] Antonio Agresti, Sara Pescetelli, Lucio Cinà, Dimitrios Konios, George Kakavelakis, Emmanuel Kymakis, Aldo Di Carlo, Efficiency and stability enhancement in perovskite solar cells by inserting lithium-neutralized graphene oxide as electron transporting layer, Adv. Funct. Mater. 26 (2016) 2686–2694.
[24] F. Giordano, A. Abate, J.P. Correa Baena, M. Saliba, T. Matsui, S.H. Im, S. M. Zakeeruddin, M.K. Nazeeruddin, A. Hagfeldt, M. Graetzel, Enhanced electronic properties in mesoporous Tio2 via lithium doping for high-efficiency perovskite solar cells, Nat. Commun. 7 (2016) 10379.
[25] C. Liu, Y. Yang, Y. Ding, J. Xu, X.L. Liu, B. Zhang, J.X. Yao, T. Hayat, A. Alsaedi, S. Y. Dai, High-efficiency and uv-stable planar perovskite solar cells using a low-temperature, solution-processed electron-transport layer, Chemsuschem 11 (2018) 1232–1237.
[26] Yi Yang, Huirong Peng, Cheng Liu, Zulqarnain Arain, Yong Ding, Shuang Ma, Xiaolong Liu, Tasawar Hayat, Ahmed Alsaedi, Songyuan Dai, Bi-functional additive engineering for high-performance perovskite solar cells with reduced trap density, J. Mater. Chem. 7 (2019) 6450–6458.
[27] Y. Yang, C. Liu, Y. Ding, Z. Arain, S. Wang, X. Liu, T. Hayat, A. Alsaedi, S. Dai, Eliminating charge accumulation via interfacial dipole for efficient and stable perovskite solar cells, ACS Appl. Mater. Interfaces 11 (2019) 34964–34972.
[28] Cheng Liu, Molang Cai, Yi Yang, Zulqarnain Arain, Yong Ding, Xiaoqiang Shi, Pengju Shi, Shuang Ma, Tasawar Hayat, Ahmed Alsaedi, Jihuai Wu, Songyuan Dai, Guozhong Cao, A C60/Tiox bilayer for conformal growth of perovskite films for Uv stable perovskite solar cells, J. Mater. Chem. 7 (2019) 11086–11094.
[29] Gon Namkoong, Abdullah A. Mamun, Tanzila Tasnim Ava, Impact of Pcbm/C60 electron transfer layer on charge transports on ordered and disordered perovskite phases and hysteresis-free perovskite solar cells, Org. Electron. 56 (2018) 163–169.